Dynamics of Solar and Stellar Convection Zones and Atmospheres
Proceedings IAU Symposium No. 365, 2024
A. V. Getling & L. L. Kitchatinov, eds.
doi:10.1017/S1743921323005392

Chromospheric activities of pre-main-sequence stars

Mai Yamashita[1], Yoichi Itoh[1], Yuhei Takagi[2] and Yumiko Oasa[3]

[1]Nishi–Harima Astronomical Observatory, Center for Astronomy, University of Hyogo, 407-2 Nishigaichi, Sayo, Sayo, Hyogo, Japan
email: yamashita@nhao.jp

[2]Subaru Telescope, National Astoronomical Observatory of Japan, 650 North A'ohoku Place, Hilo, HI 96720, U.S.A.

[3]Faculty of Education, Saitama University, 255 Shimo–Okubo, Sakura, Saitama, Saitama, Japan

Abstract. We investigated chromospheric activities of pre-main-sequence (PMS) stars. First, we studied the Ca II infrared triplet emission lines with Subaru/HDS and other spectroscopic instruments. Most PMS stars have narrow Ca II lines whose intensities are as large as the maximum of the zero-age main-sequence (ZAMS) stars. The chromosphere of PMS stars is suggested to be filled by the Ca II emitting region. Second, we found many faint chromospheric emission lines such as Mg I and Fe I for more than half of the ZAMS stars. Third, we searched the periodic light variation caused by a starspot for the 26 PMS stars. Their *TESS* light variations and Ca II emission line strengths show the positive correlation, and are located on the extensions of the superflare stars. In summary, PMS stars have very active chromosphere driven by strong dynamo process due to the fast rotation and the long convection timescale.

Keywords. stars: pre-main sequence, stars: chromospheres, stars: activity, techniques: spectroscopic, techniques: photometric

1. Introduction

Chromosphere is the region between photosphere and corona. The temperature of the chromosphere gradually increases with radial distance to the photosphere. In an active chromospheric region, atoms emit permitted lines such as Hα and Ca II. It is claimed that chromospheric activity is driven by the magnetic field, which is generated by the dynamo process.

For main-sequence stars, chromospheric activity is often discussed in relation to stellar rotation. It is claimed that chromospheric activity is driven by the magnetic field, which is generated by the dynamo process. Wilson (1978) showed that chromospheric activity analogous to that associated with the solar magnetic activity cycle is ubiquitous in stars along the lower main-sequence. As mentioned in Noyes et al. (1984), rotation is not the only parameter related to the dynamo process, but the stellar mass, spectral type, depth of convection zone, and convective turnover time (τ_c) are also related to the process. Rossby number (N_R) involves these five parameters, which is defined as

$$N_R \equiv \frac{\text{rotational period } P}{\text{convective turnover time } \tau_c}, \quad (1)$$

where P is the stellar rotational period. According to standard dynamo theory in Parker (1955), the magnetic activity at the stellar surface is getting stronger with increasing rotation speed and strength of differential rotation.

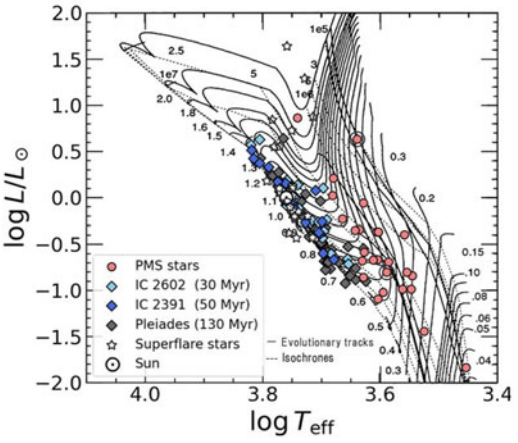

Figure 1. HR diagram of our targets. The circles, diamonds, star symbols, and odot represent the PMS stars, ZAMS stars in the three open clusters, superflare stars, and the Sun.

Marsden et al. (2009) investigated Ca II infrared triplet (IRT; $\lambda 8498, 8542, 8662$ Å) emission lines of ZAMS stars in young open clusters, IC 2391 and IC 2602. The objects having smaller the Rossby number tend to show stronger emission lines. For the stars with $\log N_{\rm R} \geq -0.8$, the ratio of the surface flux of the Ca II IRT emission line to the stellar bolometric luminosity, R' decreases with increasing $N_{\rm R}$ (the unsaturated regime). For the stars with $\log N_{\rm R} \leq -0.8$, $R'_{\rm IRT}$ is constant (the saturated regime).

Because PMS stars are fast rotators (Gallet & Bouvier 2013), they are expected to have high dynamo activities. We suppose that the low-mass PMS stars are fully-convective and have the large-scale starspots.

2. Observations and Data reduction

We investigated the Ca II IRT for 60 PMS stars (Fig. 1; $10^5 - 10^8$ yr, $0.035 - 2.5\,{\rm M}_\odot$), being associated with four molecular clouds or five moving groups. The medium- and high-resolution spectroscopy were conducted with 2 m Nayuta Telescope/MALLS at Nishi–Harima Astronomical Observatory and Subaru/HDS. Archival data obtained with the Keck/HIRES, VLT/UVES, and VLT/X-Shooter were also used. A detailed description of the data reduction methods used here is presented in Yamashita et al. (2020).

We also investigated the Mg I line of F, K, G type 52 ZAMS stars by using 3.9 m Anglo-Australian Telescope (AAT)/the University College London Echelle Spectrograph (UCLES) archive spectra. The PI is S. C. Marsden, date of the observations are 2000-03-17, 18, 19, 2001-01-06, 07, 08, and 2001-02-11, 12. The wavelength coverage was between 3522 Å and 9386 Å. The integration time for each object was between 300 s and 1200 s. A detailed description of the observations is presented in Marsden et al. (2009), and that description of the data reduction methods used here is presented in Yamashita et al. (2022a). The Mg I emission component is always buried by the photospheric absorption as shown in Fig. 2.

In this study, inactive stars with a spectral type similar to that of the target were used as template stars. For the correction of the rotational broadening, the spectra of the template stars were convolved with a Gaussian kernel to match the width of the photospheric absorption lines of each object. By using high S/N spectra of inactive field stars, we carefully subtracted the photospheric absorption component. We considered that the subtraction was reliable if nearby faint photospheric absorption lines, such as

https://doi.org/10.1017/S1743921323005392 Published online by Cambridge University Press

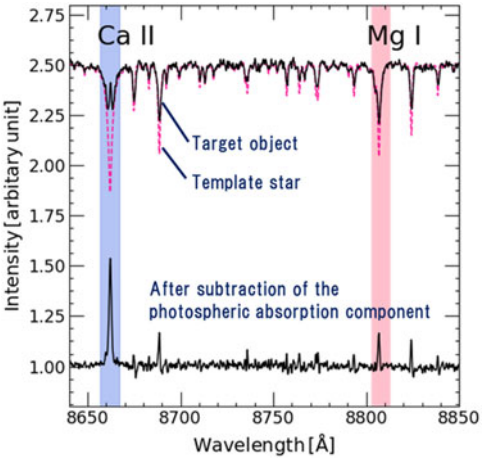

Figure 2. The procedures of the spectral subtaction of the photospheric component for the PMS star, RECX 11

Ni I, Mn I, V I, and Ti I, disappeared in the spectrum after the subtraction. Finally, we measured the equivalent widths (EQW) of the Mg I emission line. Before measuring the EQWs, the continuum component of the spectra was added to unity. To obtain the EQWs of the Mg I emission lines, the area of the emission profile was directly integrated. The typical EQW errors were estimated by multiplying the standard deviation of the continuum by the wavelength range of the Mg I emission line of the five ZAMS stars.

The PMS stars and ZAMS stars were also observed by *TESS*. We retrieved the Presearch Data Conditioning Simple Aperture Photometry (PDCSAP) fluxes for each PMS star from the Multimission Archive at the Space Telescope Science Institute. We searched periodicity of the light curve then obtained its amplitude. For ZAMS stars, we conducted principal component analysis using ELEANOR, an open-source tool for extracting light curves from *TESS* full-frame images (Feinstein et al. 2019). We calculated the standard deviation of the flux, σ_1, and removed the flux data points greater than $3\sigma_1$ above the average. We searched for periodic signals by conducting Lomb–Scargle (Scargle 1982) periodogram analysis. For each object, the period of the light curve was determined. The amplitudes of the light curves were calculated by taking the 90th percentile flux and subtracting it from the 10th percentile flux. The detail is described in Yamashita et al. (2022a).

3. Result

Seven PMS stars have broad emission lines of Ca II λ8498 Å (FWHM $> 100\,\mathrm{km\cdot s^{-1}}$), while most PMS stars exhibit narrow emission lines (FWHM $\leq 100\,\mathrm{km\cdot s^{-1}}$). The emission lines of DG Tau, DL Tau, and DR Tau are broad and strong (EQW ~ 50 Å), while those of RY Tau, SU Aur, RECX 15, and RX J1147.7-7842 are broad but not strong (EQW < 10 Å). All EQWs of the narrow emission lines are weaker than 5 Å.

Before subtracting the photospheric absorption component, the Mg I emission component is always buried by the photospheric absorption. As a result of the data reduction, the Mg I line is detected as an emission line in 45 ZAMS stars. The Mg I line of these ZAMS stars shows narrow emission, indicative of chromospheric origin. Their EQWs range from 0.02 Å to 0.63 Å. The Mg I emission lines of 33 ZAMS stars have EQWs less than 0.1 Å. 5 ZAMS stars do not show the Mg I line in emission or absorption, but like simply continuum component.

https://doi.org/10.1017/S1743921323005392 Published online by Cambridge University Press

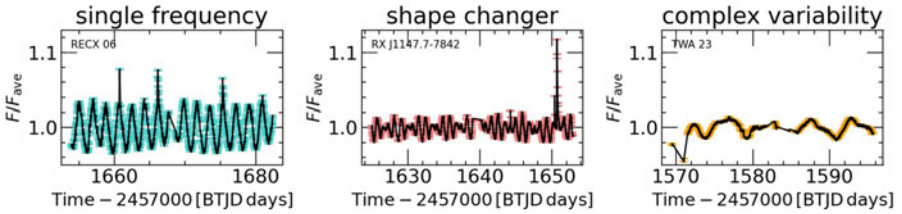

Figure 3. Three examples of the *TESS* light curves of PMS stars. The three features of the light curve, a) single frequency, b) possible shape changer, and c) complex variability, are presented.

For 26 PMS stars, the amplitudes of the light curves are $0.001 - 0.552$ mag. Fig. 3 shows three examples of light curves of the PMS stars. For the 26 PMS stars and 33 ZAMS stars in IC 2391 and IC 2602, we categorized the light curves into the following groups:

a) Single frequency: the star has a single period. A single spot or spot group is interpreted as rotating into and out of view.
b) Possible shape changer: subcategory of type a) single frequency. The star usually has a single period. Shape of the light curve may change in the observational period.
c) Complex variability; the light curve has periodicity but seems complex. It is considered that the star has multiple spot groups.

We categorized 11 PMS stars and 16 ZAMS stars as type a) single frequency, 4 PMS stars and 11 ZAMS stars as type b) possible shape changer, and 11 PMS stars and 5 ZAMS stars as type c) complex variability.

4. Discussion

Q1. How related the chromospheric activity of PMS stars with their rotation ?

We examined the relationship between R' of the Ca II IRT emission line, and $N_{\rm R}$ of the 60 PMS stars (Fig. 4). For calculating $N_{\rm R}$, we estimated $\tau_{\rm c}$ of the PMS stars using pre-main sequence evolutionary tracks presented in Jung & Kim (2007). In this track, $\tau_{\rm c}$ of low-mass stars near the main sequence was not calculated. For such objects, we applied the approximation of Noyes et al. (1984). A detailed description of the calculation of $N_{\rm R}$ and R' is presented in Yamashita et al. (2020).

Fig. 4 shows the relationship between Rossby number and the Ca II emission line strength of PMS stars. Only three PMS stars show broad and strong emissions, indicative of large mass accretion. Most of the PMS stars have narrow and weak emissions.

Fig. 4a shows the objects with the single frequency. All of their Ca II IRT emission lines have $R' \sim 10^{-4.2}$, which is as large as the maximum R' of ZAMS stars (Marsden et al. 2009). The PMS stars have $N_{\rm R} < 10^{-0.8}$ and constant R' against $N_{\rm R}$; i.e., the Ca II IRT emission lines of the PMS stars are saturated. The chromosphere of these stars is considered to be completely filled by the active region. We consider that the objects have stable spot because they show sinusoidal light curves. This indicates that their chromospheric activity is induced by the dynamo process.

In Fig. 4c, we plotted the PMS stars with complex variability. They tend to have large Rossby numbers. We consider that small spots on the photosphere cause the irregular variability.

https://doi.org/10.1017/S1743921323005392 Published online by Cambridge University Press

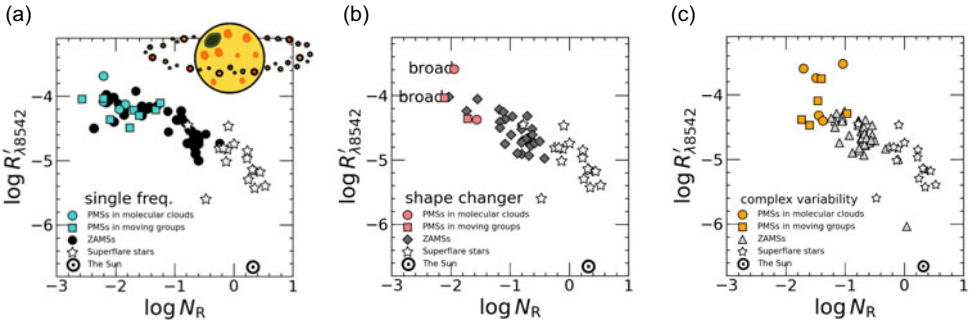

Figure 4. Ca II emision line strength, $R'_{\lambda 8542}$, as a function of the Rossby number, N_R (Yamashita et al. 2020, 2024 in prep.). The colored symbols represent PMS stars. The filled circles in Fig. 4a, gray diamonds in Fig. 4b, open triangles in Fig. 4c show the ZAMS stars with single frequency, the possible shape changer ZAMS stars, ZAMS stars and complex variability, respectively. The star symbols and odot denote the superflare stars and the Sun (Notsu et al. 2015).

Q2. How about optically thinner emission lines ?

Because all R' of Ca II IRT emission lines were saturated against N_R, it was not possible to estimate the appropriate τ_c model for the PMS stars. PMS stars with unsaturated chromospheric emission lines should be investigated.

We examined the relationship between the ratio of the surface flux of the Mg I emission line to the stellar bolometric luminosity, R'_{MgI}, and N_R of the ZAMS stars. In this work, we refereed N_R calculated by Marsden et al. (2009) for ZAMS stars. They used P for 21 ZAMS stars or $v \sin i$ for 31 ZAMS stars. We calculated R' for the Mg I emission line. For calculating the surface flux of the line F', a bolometric continuum flux per unit area at a stellar surface, F, was calculated at first. We used the i-band mag (the AB system) of the UCAC4 Catalogue Zacharias et al. (2013) and Marsden et al. (2009). F is given as

$$\log \frac{f}{f_0} = -\frac{2}{5} \times m_{i*}, \tag{2}$$

$$F = f \times \left(\frac{d}{R_*} \right)^2, \tag{3}$$

where f is the bolometric continuum flux of the object per unit area as observed on the Earth. m_{i*} is the apparent magnitude of the object in the i-band. The bolometric continuum flux per unit area under $m_i = 0$ mag (the AB system) condition, f_0, is $1.852 \times 10^{-12}\,\mathrm{W \cdot m^{-2} \cdot \AA^{-1}}$ Fukugita et al. (1996). d denotes the distance of an object from the Earth (*Gaia* DR2: Bailer–Jones et al. 2018). R_* is the stellar radius estimated using Stefan–Boltzmann's law with the photospheric luminosity, and T_{eff} of the objects in *Gaia* DR2 and Marsden et al. (2009). F was multiplied by the EQW of the Mg I emission lines.

$$F' = F \times \mathrm{EQW}, \tag{4}$$

For calculating R', F' are divided by σT_{eff}^4.

$$R' = \frac{F'}{\sigma T_{eff}^4}, \tag{5}$$

where σ is Stefan–Boltzmann's constant. The dependence of the surface flux upon the T_{eff} of the objects is eliminated by this calculation.

https://doi.org/10.1017/S1743921323005392 Published online by Cambridge University Press

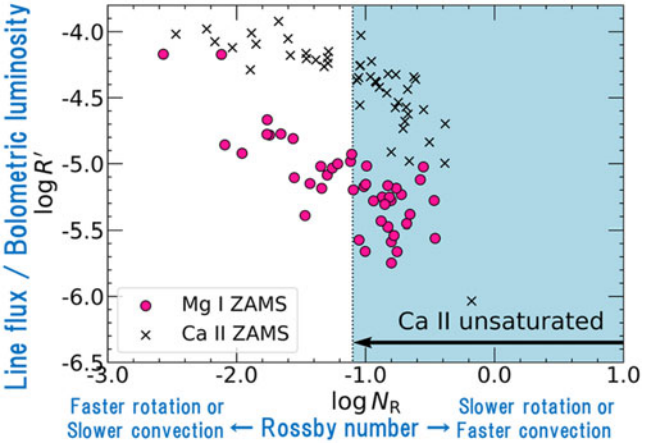

Figure 5. Relationship between ratio of surface flux of Mg I emission line (λ8807 Å) to stellar bolometric luminosity $R'_{\rm MgI}$ and Rossby number $N_{\rm R}$ of ZAMS stars (circles). Cross symbols represent $R'_{\lambda 8542}$, which is ratio of surface flux of Ca II λ8542 Å line to stellar bolometric luminosity, of ZAMS stars. (Yamashita et al. 2022a)

Fig. 5 shows the relationship between $R'_{\rm MgI}$ and $N_{\rm R}$ of the ZAMS stars. We found that the Mg I line is still not saturated in the region of $10^{-1.8} < N_{\rm R} < 10^{-0.8}$, which is the saturated region for Ca II IRT emission lines. According to the discussion by Marsden et al. (2009), the chromospheric saturation is suggested to be caused by the similar to coronal saturation. Suppose if the emitting region of Ca II are completely filled, the unsaturation of the Mg I emission line suggests that the area of the Mg I emitting region may be smaller than that of Ca II. Otherwise Mg I is optically thinner than Ca II. We conclude that the optically thin Mg I enables us to evaluate the strength of the dynamo activity for many object having strong magnetic field.

Q3. For PMS stars, how related the starspot coverage with the chromosphere ?

Notsu et al. (2015) indicated that the Sun and superflare stars show a rough positive correlation between the amplitude of the light curve and the $r_0(8542)$ index, the residual core flux normalized by the continuum level at the line core of the Ca II IRT. They claimed that the magnetic field strengths of superflare stars are higher than that of the Sun.

We investigated the amplitude of the light curve and $R'_{\lambda 8542}$ for PMS stars and ZAMS stars (Fig. 6). The ZAMS stars with a large light curve amplitude have large $R'_{\lambda 8542}$. The $R'_{\lambda 8542}$ and light curve amplitudes of ZAMS stars are approximately two orders of magnitude larger than those of the Sun. We also found that the ZAMS stars are located on the extensions of the superflare stars (Notsu et al. 2015). This result suggests that superflare stars link the properties of the Sun to those of the ZAMS stars of ages between 30 and 120 Myr.

Objects with different types of light curves seem to be unevenly distributed in Fig. 6, as represented by the colors of the symbols. Fig. 6a shows the PMS stars and ZAMS stars with single frequency. The ZAMS stars with single frequency have larger light curve amplitudes and larger $R'_{\lambda 8542}$ compared with other light curve type ZAMS stars. The PMS stars with single frequency show large light curve amplitudes and large $R'_{\lambda 8542}$. We consider that they have enormous spots of one to ten % of the surface, as well as bright chromospheric emission lines.

https://doi.org/10.1017/S1743921323005392 Published online by Cambridge University Press

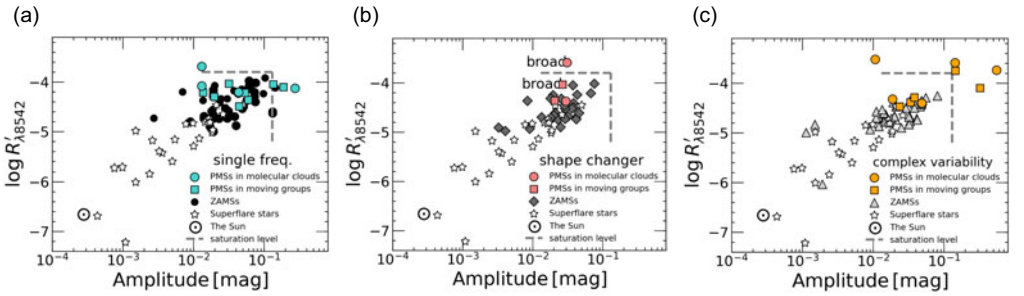

Single frequency objects Shape changer Complex variability

Figure 6. $R'_{\lambda 8542}$ as a function of the light curve amplitude of PMS stars (the colored circles and squares; this work), ZAMS stars (the black circles, gray diamonds, and gray triangles; Yamashita et al. 2022b), superflare stars (star marks; Notsu et al. 2015), and the Sun (odot; Notsu et al. 2015).

The ZAMS stars with complex variability have smaller light curve amplitudes and smaller $R'_{\lambda 8542}$ compared with other type ZAMS stars (Fig. 6c). A part of PMS stars are located near the ZAMS stars. We consider that they have small spots.

5. Acknowledgments

M. Y is supported by JSPS KAKENHI grant number 23KJ1855, and Y. I. is supported by JSPS KAKENHI grant number 22K03677. This paper includes data collected with the TESS mission, obtained from the MAST data archive at the Space Telescope Science Institute (STScI).

References

Bailer–Jones, C. A. L., Rybizki, J., Fouesneau, M., Mantelet, G., & Andrae, R. 2018, ApJ., 156, 58
Feinstein, A. D., Montet, B. T., Foreman–Mackey, D., et al. 2019, PASP, 131
Folsom et al. 2018, MNRAS, 474, 4956
Fleck, B., Deubner, F.-L., Maier, D., & Schmidt, W. 1994, IAU Symp, 154, 65
Fukugita, M., Ichikawa, T., Gunn, J. E., et al. 1996, AJ, 111, 1748
Gallet, F., & Bouvier, J. 2015, A&A, 577, 1
Hamann, F., & Persson, S. E. 1992a, Astrophys. J. Suppl., 82, 247
Jung, Y. K., & Kim, Y.-C. 2007, J. Astron. Space Sci., 24, 1
Linsky, J. L. 2017, Annu Rev Astron Astrophys, 55, 159
Marsden, S. C., Carter, B. D., & Donati, J.-F. 2009, MNRAS, 399, 888
Neuhauser, R., Strerzik, M. F., Schmitt, J. H. M. M., Wichmann, R., & Krautter, J. 1995, Astron. Astrophys., 297, 391
Notsu, Y., Honda, S., Maehara, H., et al. 2015, PASJ, 67, 1
Noyes, R. W., Hamann, F. W., Baliunas, S. L., & Vaughan, A. H. 1984, AJ, 279, 763
Parker, E. N. 1955, ApJ, 122, 293
Rebull, L. M., Stauffer, J. R., Bouvier, J., et al. 2016, AJ, 152, 114
Scargle, J. D. 1982, AJ, 263, 835
Skelly, M. B., Donati, J. F., Bouvier, J., et al. 2010, MNRAS, 403, 159
Stelzer, B., Fernandez, M., Costa, V. M., et al. 2003, A&A, 411, 517
Vernazza, J. E., Avrett, E. H., & Loeser, R. 1981, ApJS, 45, 635
Wilson, O. C. 1978, ApJ, 226, 379
Yamashita, M., Itoh, Y., & Takagi, Y. 2020, PASJ, 72, 80
Yamashita, M., & Itoh, Y. 2022a, PASJ, 74, 557
Yamashita, M., Itoh, Y. & Oasa, Y., 2022b, PASJ, 74, 1295
Zacharias, N., Finch, C. T., Girard, T. M., et al. 2013, Astrophys. J., 145, 1

https://doi.org/10.1017/S1743921323005392 Published online by Cambridge University Press